Acta Cryst. (1973). A29, 545

Direct Determination of X-ray Phases for Tobacco Mosaic Virus Protein using Non-crystallographic Symmetry

BY ANTHONY JACK *

M.R.C. Laboratory of Molecular Biology, Hills Road, Cambridge, England

(*Received* 11 *December* 1972; *accepted* 6 *April* 1973)

The basic structural unit of tobacco mosaic virus (TMV) protein crystals is a ring of seventeen identical subunits. This non-crystallographic 17-fold symmetry has been used to determine signs of the X-ray reflexions in the centrosymmetric *hk*0 projection, in two different but related ways. The results are compared with those obtained by Gilbert [Ph. D. Thesis (1970), Univ. of Cambridge] using the method of single isomorphous replacement (SIR), and are shown to agree well for reflexions with $(h+k)$ even. Owing to the special positions of the bound heavy atoms, reliable signs have not hitherto been available for reflexions with $(h+k)$ odd. Evidence is presented to show that those obtained from the non-crystallographic symmetry are essentially correct.

Introduction

Tobacco mosaic virus (TMV) is the most thoroughly studied of the helical viruses. A single virus particle, of length about 3000 Å, and diameter 180 Å consists of a central core of ribonucleic acid (RNA) surrounded by some 2130 identical helically arranged protein subunits (Watson, 1954; Franklin & Holmes, 1958). It is possible to separate the protein subunits from the RNA core, and it is found that the protein reaggregates in several different ways, depending on *p*H, ionic strength *etc.* (Caspar, 1963; Klug & Durham, 1971). One of the stable aggregates near neutral *p*H is a 'disc', in which two rings of subunits are superimposed head to tail (Finch & Klug, 1971).

Finch, Leberman, Yu-shang & Klug (1966) succeeded in crystallizing the coat protein, and showed from electron micrographs that the crystals were based on the discs of subunits mentioned above. Low-angle screenless precession photographs clearly showed rings of 34 equally spaced regions of strong intensity, indicating that each ring of the disc contained 17 subunits, and close examination of the micrographs showed the discs to have 17-fold symmetry. More recently, Crowther & Amos (1971) have used a harmonic analysis technique to show that the strongest harmonic component in the micrographs is that corresponding to 17-fold rotation. This, together with the X-ray evidence, leaves no doubt that the disc has 17-fold symmetry.

Further X-ray studies (Finch *et al.*, 1966; Gilbert, 1970) have shown the crystals to have space-group symmetry $P22_12_1$ with lattice parameters $a=228{\cdot}2\pm{\cdot}5$, $b=223{\cdot}9\pm{\cdot}5$, $c=174{\cdot}3\pm{\cdot}5$ Å. The crystallographic asymmetric unit consists of a disc of two superimposed rings (arranged in a polar manner but with different azimuthal orientations) whose local 17-fold axis is nearly parallel to the crystallographic *z* axis.

* Present address: Gibbs Laboratory, Harvard University, 12 Oxford St., Cambridge, Mass. 02138, U.S.A.

Fig. 1 shows the crystal packing arrangement, from which it can be seen that in the *z*-axis projection the discs stack in pairs, and also that there is some overlap between neighbouring stacks. Gilbert (1970) has made an extensive study of these crystals. He has used the method of single isomorphous replacement (SIR), with a methylmercury derivative, to obtain signs for the X-ray reflexions corresponding to the three centrosymmetric projections of the protein. During least-squares refinement of the mercury-atom coordinates deduced from difference Patterson projections, it became clear that the local 17-fold axes were tilted some $1\frac{1}{2}°$ off **z** towards the *y* axis, and also that the stacks were not centred exactly at 0,0,0 and $\frac{1}{2},\frac{1}{2},\frac{1}{2}$, but that each disc of the stack had a small displacement in the **y** direction. These small deviations from the ideal arrangement have been ignored in the work described below.

All the X-ray intensities used in this work were measured by Dr P. F. C. Gilbert (Gilbert, 1970) using $7\frac{1}{2}°$ precession photographs and a computer-controlled flying-spot densitometer. Amplitudes measured in this way are generally accurate to within less than 5%, and although the effect of amplitude errors has not been studied for this particular case, model calculations have shown that this level of error is quite acceptable, and has little effect on the solution of the phase equations.

Exploitation of the non-crystallographic symmetry

Rossmann & Blow (1963, 1964) were the first to show that if the rotation and translation parameters relating crystallographically independent subunits are known, then it is possible to determine a set of X-ray phases subject to the constraint that the electron-density distributions in these subunits be identical. These ideas have been generalized and further extended by Main & Rossmann (1966), Main (1967) and Crowther (1967, 1969), who showed that the phase relationships could conveniently be written in matrix notation as

$$\mathbf{HF}=\mathbf{F} \qquad (1)$$

where **F** is a column vector of complex structure factors, and **H** is a Hermitian matrix whose elements depend only on the shape and size of the subunits and the rotations and translations relating them.

Crowther's derivation assumes that it is possible to define an 'envelope' which contains all the significant electron density in one subunit, and none from its neighbours. If, however, the non-crystallographic symmetry is pure rotational, a simpler expression for the matrix element can be derived (Crowther, 1968) by defining an envelope U which contains all the significant density in the asymmetric unit. Such an envelope must, of course, have point-group symmetry at least as high as that of the subunit aggregate. An argument similar to that given by Main & Rossmann (1966), and by Crowther (1967), leads to a set of equations of the form

$$F_{\mathbf{h}}=\frac{1}{n}\sum_{\mathbf{p}} F_{\mathbf{p}} \sum_{j=1}^{n}\int_{U} \exp 2\pi i(\mathbf{h}\,.\,\mathbf{x}_j-\mathbf{p}\,.\,\mathbf{x}_1)\mathrm{d}\mathbf{x}_1 \qquad (2)$$

where n is the number of subunits and

$$\mathbf{x}_j=\mathbf{C}_j\mathbf{x}_1+\mathbf{d}_j, \qquad (3)$$

$\mathbf{C}_j$ and $\mathbf{d}_j$ being appropriate rotation matrices and translation vectors defining the non-crystallographic symmetry.

The integral (Patterson, 1939; Rossmann & Blow, 1962) may be written as

$$\frac{U}{V} G(2\pi R_j a) \exp\{2\pi i(\mathbf{h}-\mathbf{p})\,.\,\mathbf{S}\}$$

where V is the cell volume, G is the amplitude of the Fourier transform of the envelope volume U, R_j is the reciprocal distance $|\mathbf{h}\,.\,\mathbf{C}_j-\mathbf{p}|$, $\mathbf{S}$ is a vector from the origin to the molecular centre, and a is the radius of the envelope. Thus finally we have

$$F_{\mathbf{h}}=\frac{U}{nV}\sum_{\mathbf{p}} F_{\mathbf{p}} \exp\{2\pi i(\mathbf{h}-\mathbf{p})\,.\,\mathbf{S}\} \sum_{j=1}^{n} G(2\pi R_j a)\,. \qquad (4)$$

Crowther (1969) has suggested an elegant method of solution of equation (1), based on the fact that the eigenvalues of **H** all lie between 0 and 1. Since any eigenvector of **H** corresponding to unit eigenvalue must be a solution, the vector of structure factors **F** can be considered as a combination of 'allowed' components, corresponding to these eigenvectors, together with 'non-allowed' components, these being the eigenvectors corresponding to the non-unit eigenvalues. Thus as a first approximation all the phases can be set to zero (in the absence of any better estimate), and the resulting vector **F** multiplied by **H**. This leaves unchanged the components of **F** corresponding to unit eigenvalues, and tends to remove components corresponding to the smaller eigenvalues. The phases of the new **F** vector are then combined with the observed amplitudes, and the process repeated until the mean phase change per cycle drops below some specified minimum.

Setting up the equations for TMV protein

The z-axis projection of TMV protein has plane-group symmetry *pgm*, with two discs per cell centred at $\frac{1}{4},\frac{1}{4}$ and $\frac{3}{4},\frac{3}{4}$. (Note that the origin has been shifted by $-\frac{1}{4},-\frac{1}{4}$ from that shown in Fig. 1 in order to make a centre of symmetry coincide with the crystallographic origin.) Thus the integral on the right of equation (2) must be taken over two discs, and is real because of the centrosymmetry of the projection. The function G is in this case the Fourier transform of a disc, given by

$$G(2\pi R_j a)=J_1(2\pi R_j a)/\pi R_j a$$

(see, *e.g.* James 1948, p. 399), where J_1 is a first-order Bessel function, and a the disc radius (Fig. 2). Since the crystallographic symmetry introduces no further non-crystallographic symmetry operators in reciprocal space, equation (4) becomes

$$F_{\mathbf{h}}=\frac{2cU}{nV}\sum_{\mathbf{p}} F_{\mathbf{p}} \cos\{2\pi\,(\mathbf{h}-\mathbf{p})\,.\,\mathbf{S}\} \sum_{j=1}^{n} G(2\pi R_j a)\,. \qquad (5)$$

The term $1/V$ on the right of (4) has now been replaced by c/V, since we are dealing specifically with a projection. Substituting $\mathbf{S}=\frac{1}{4},\frac{1}{4}$ into (5), and writing $\mathbf{h}=h,k,0$ and $\mathbf{p}=p,q,0$, we find

$$F_{\mathbf{h}}=\frac{2cU}{nV}\sum_{\mathbf{p}} F_{\mathbf{p}} \cos\left\{\frac{\pi}{2}(h-p+k-q)\right\} \sum_{j=1}^{n} G(2\pi R_j a)\,.$$

Two distinct cases may now arise:

(1) $(h+k)$ *and* $(p+q)$ *both even or both odd,* leading to

$$H_{\mathbf{hp}}=\pm\frac{2cU}{nV}\sum_{j=1}^{n} G(2\pi R_j a)\,.$$

(2) $(h+k)$ *even and* $(p+q)$ *odd, or* $(h+k)$ *odd and* $(p+q)$ *even.* In both cases, $(h-p+k-q)$ is odd, and $H_{\mathbf{hp}}\equiv 0$.

Hence the reflexions fall into two parity groups, and only pairs of reflexions belonging to the same parity group are related by the non-crystallographic symmetry equations.

The derivation above takes no account of the slight tilts and displacements of the discs mentioned in the Introduction, although these are unlikely to have much effect on the signs, especially at low resolution. A po-

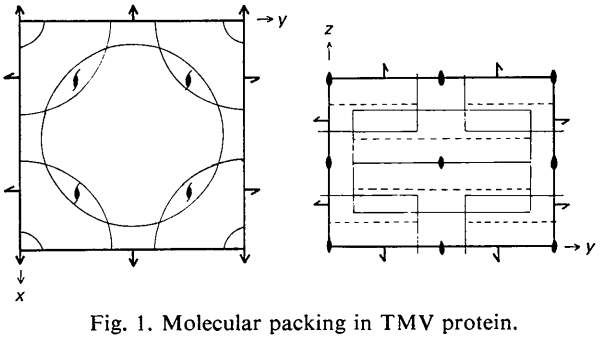

Fig. 1. Molecular packing in TMV protein.

tentially more serious problem is the overlap which occurs if the molecules are assumed to be discs of radius 90 Å. A method of avoiding this difficulty is discussed in a subsequent section, although the results show that in practice the effect of overlap is not as important as might have been supposed.

The effect of truncation of the *G* function

The function $G(2\pi Ra)=J_1(2\pi Ra)/(\pi Ra)$ oscillates like an attenuated cosine wave, but never dies away to zero (Fig. 2), so that in theory the summation in equation (5) must be taken over the whole of reciprocal space. Clearly this is impractical, and it is necessary to truncate the summation over **p** at some stage by setting an upper limit to the allowed arguments of *G*. Tollin & Rossmann (1966) have shown that this truncation of the *G* table is equivalent to a series termination effect in real space. If we consider the electron density in the cell to be multiplied by a shape function $g(x)$ (the Fourier transform of *G*), such that

$$\varrho'(x)=\varrho(x)g(x)$$

then ideally this function *g* must everywhere have the value 0 or 1 if $\varrho'\equiv\varrho$. Because of the series termination,

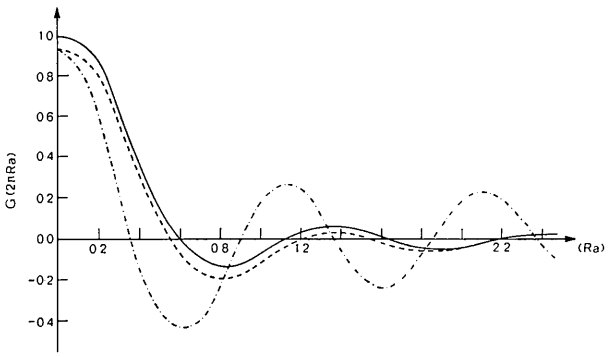

Fig. 2. The *G* function and its first derivative. (——): disc, radius *a*; (-----): annulus, radii *a* and 0·22*a*; (-·-·-): $\partial G/\partial a$ for annulus.

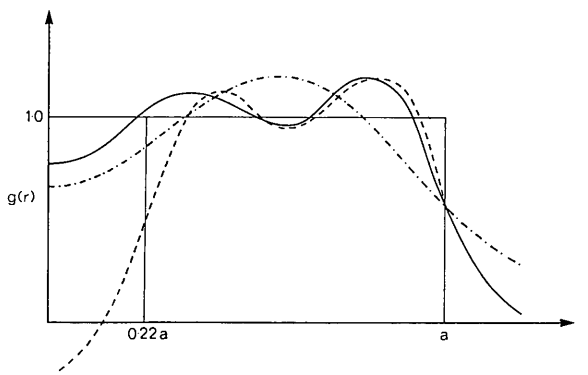

Fig. 3. Shape functions obtained by Fourier–Bessel inversion of the truncated *G* function. (——): disc, $(Ra)_{max}=2{\cdot}5$; (-·-·-): disc, $(Ra)_{max}=1{\cdot}25$; (-----): annulus, $(Ra)_{max}=2{\cdot}5$.

however, the function *g* does not drop abruptly to zero at its boundary, but instead decreases more slowly, and may be significantly less than unity at radii less than *a*. For example, Fig. 3 shows some effective shape functions calculated by Fourier–Bessel inversion of the truncated *G* function

$$g(r)=2\pi\int_0^{R_{max}} G(2\pi Rr)J_0(2\pi Rr)R\,dR$$

with maximum allowed arguments of $Rr=2{\cdot}5$ and 1·25. This series termination effect is worsened by the computationally necessary practice of using only the largest terms of the matrix **H**. Since this tends to choose terms which are dominated by a few large *G* values, the effective truncation of *G* may be even sharper than expected, with a consequently more serious effect on the shape function. The result of this is that the phases generated by the method, when combined with the observed amplitudes, tend to give low weight to the electron density near the envelope boundary; indeed, this effect is clear in Crowther's (1969) Fourier map of triaminotrinitrobenzene. In the centrosymmetric case, at least, one solution to this problem is to overestimate the value of the molecular radius. This then leads to full-weight density out to the edge of the envelope, at the expense of some low-weight overlap between neighbouring envelopes. A reasonable assumption is that the optimum molecular radius (for given maximum *G* argument, number of terms *etc.*) is that which minimizes the root-mean-square lack of closure of the equations (5), since we are seeking to fill as much of the cell with density as is consistent with no overlap between adjacent envelopes. Tests with a two-dimensional model structure indicated that this is a valid procedure, and the method finally adopted was to perform a least-squares refinement of the envelope radius alternately with cycles of sign determination.

Refinement of envelope parameters

We want to adjust the disc radius, *a*, so as to minimize the squared lack of closure

$$\sum_{\mathbf{h}}\varepsilon_{\mathbf{h}}^2=\sum_{\mathbf{h}}(F_{obs}-|F_{calc}|)^2$$

where F_{obs} is the observed amplitude for reflexion **h**, and F_{calc} the value obtained by summing the right-hand side of (4). Assuming that ε is a linear function of *a*, this leads to normal equations

$$\sum_{\mathbf{h}}\left\{\frac{\partial|F_{calc}|}{\partial a}\right\}^2\Delta a=\sum_{\mathbf{h}}\left\{\frac{\partial|F_{calc}|}{\partial a}\right\}\varepsilon_{\mathbf{h}}\,.$$

Now since

$$F_{\mathbf{h}(calc)}=\sum_{\mathbf{p}}H_{\mathbf{hp}}F_{\mathbf{p}}$$

we have

$$\frac{\partial|F_{calc}|}{\partial a}=\text{sign}\,(F_{\mathbf{h}})\sum_{\mathbf{p}}\frac{\partial H_{\mathbf{hp}}}{\partial a}F_{\mathbf{p}}$$

where, from (4)

$$\frac{\partial H_{hp}}{\partial a} = \frac{1}{n} \exp\{2\pi i(\mathbf{h}-\mathbf{p}) \cdot \mathbf{S}\} \sum_{j=1}^{n} \frac{\partial}{\partial a}\left\{\begin{matrix} U \\ V \end{matrix} G(2\pi R_j a)\right\} .$$

Putting $U=\pi a^2$, $G(x)=2J_1(x)/x$, and using the relationship

$$\frac{\mathrm{d}}{\mathrm{d}x}(J_n(x)/x^n) = -J_{n+1}(x)/x^n,$$

we find

$$\frac{\partial H_{hp}}{\partial a} = \frac{2U}{naV} \exp\{2\pi i(\mathbf{h}-\mathbf{p}) \cdot \mathbf{S}\} \times \sum_{j=1}^{n} \left\{G(2\pi R_j a) - J_2(2\pi R_j a)\right\} .$$

Hence $\partial\mathbf{H}/\partial a$ is calculable, and from it Δa. In practice, the signs are determined a few at a time, working out from the origin of reciprocal space (Main, 1967), and application of this least-squares procedure after each block of signs has been determined rapidly leads to a stable value of a.

Direct calculation of the allowed eigenvectors

Although the phasing method described above depends on the eigenvalue properties of the matrix **H**, these eigenvalues and their eigenvectors are never explicitly calculated. If we knew the eigenvectors, then an alternative approach to the problem would be possible, since the transform of the structure of interest can be expressed as a linear combination of those eigenvectors corresponding to unit eigenvalue. In Crowther's notation

$$\mathbf{F} = \sum_{j=1}^{m} \mu_j \mathbf{u}_j$$

where the $\mathbf{u}_j$ are the m allowed eigenvectors, μ_j their (real) weighting factors, and **F** is the Fourier transform of the structure. **F** and **u** are in general complex, although in the problem to be discussed here they are real because of the centrosymmetry of the projection. Since only intensities (**FF*** or $|F|^2$) are known at the start of the investigation, Crowther suggested that the μ_j could be determined by solving the set of quadratic equations

$$F_h F_h^* = \sum_{j=1}^{m} \sum_{k=1}^{m} \mu_j \mu_k u_{jh} u_{kh}^*, \quad h=0,1 \ldots N ,$$

where N is the number of available X-ray observations.

Owing to the difficulty of solving such a set of equations, this method of determining the phases was not pursued. However, an alternative method of determining the μ_j exists, which is mathematically equivalent to the iterative phase determination scheme finally adopted by Crowther (1969) and described above. Let us assume that we know the m allowed eigenvectors **u**. Then we can construct an $N \times m$ matrix, **A**, whose columns are these eigenvectors. Then since the **u** form an orthonormal set, and $\mathbf{F} = \sum_{j=1}^{m} \mu_j \mathbf{u}_j$, we have

$$\mathbf{F} = \mathbf{A}\mu$$

and

$$\mu = \tilde{\mathbf{A}}^* \mathbf{F} .$$

From this we see that

$$\mathbf{F} = \mathbf{A}\tilde{\mathbf{A}}^* \mathbf{F} \tag{6}$$

and $\mathbf{A}\tilde{\mathbf{A}}^*$ is an $N \times N$ matrix, m of whose eigenvalues are unity while the remainder are identically zero. Thus as far as determining the phases is concerned, $\mathbf{A}\tilde{\mathbf{A}}^*$ is analogous to **H**, and we can solve (6) by a two-step iterative process:

(1) multiply the current best estimate of **F** by $\tilde{\mathbf{A}}^*$ to get μ;

(2) evaluate $\mathbf{F} = \mathbf{A}\mu$, and reset the $|\mathbf{F}|$'s to their observed values, repeating these steps until the process converges.

It is easily shown that this is equivalent to least-squares fitting, when the current phases are used on the right-hand side of the normal equations.

As in the iteration with the matrix **H**, there is no guarantee that this method (henceforth referred to as the eigenvector method) will produce the best μ_j and therefore the correct phases; indeed it is easy to write down small **A** matrices which converge to an incorrect solution if no prior phase information is introduced. Nevertheless it is to be hoped that with a large enough redundancy (*i.e.* N:m ratio) the best solution will be obtained.

The allowed eigenvectors for TMV protein

Any two-dimensional function bounded by a disc may be expanded in functions of the form

$$\psi_{nm}(r,\varphi) = J_n(k_{nm} r) \exp(in\varphi) \tag{7}$$

(*i.e.* a Fourier series in cylindrical polar coordinates). Here r and φ are real-space coordinates, J_n is the Bessel function of order n, and k_{nm} is chosen to make the mth zero of J_n fall on the edge of the disc. The ψ_{nm} form a complete set of functions periodic in φ, so that any arbitrary density inside a disc may be expressed as

$$\varrho(r,\varphi) = \sum_{n=-\infty}^{\infty} \sum_{m=1}^{\infty} \mu_{nm} \psi_{nm}(r,\varphi) .$$

If we consider a two-dimensional 'close-packed crystal' of such discs, with no restrictions on the density distribution inside the disc, then the number of eigenfunctions ψ_{nm} required to describe the structure to a given resolution is approximately twice the number of available X-ray observations. [More exactly, it is $2U/V$, corresponding to the gradient of the m,N plot as given by Crowther (1967).] In other words, the system is just determined, in the sense of having as many equations as unknowns, when the phases are known initially, that is,

there are two 'observations' per reflexion. If, however, the density inside the disc is known to possess j-fold rotational symmetry, then the only allowed eigenfunctions are those for which n is an integral multiple of j, thus reducing the number of unknowns by a factor of j. We will now derive an expression for the structure factors of TMV protein in terms of the Fourier transforms of these functions.

The eigenvector $\mathbf{u}_{nm}$ corresponding to the eigenfunction $\psi_{nm}(r,\varphi)$ can be found by Fourier–Bessel transformation:

$$\mathbf{u}_{nm}(R,\Phi)=\exp\left[in\left(\varphi+\frac{\pi}{2}\right)\right]\int_0^a J_n(k_{nm}r)\,J_n(2\pi Rr)\,2\pi r\mathrm{d}r \tag{8}$$

where R,Φ are cylindrical coordinates in reciprocal space, and a is the radius of the disc. Now since

$$\int J_n(\alpha z)J_n(\beta z)z\mathrm{d}z=\frac{z}{\alpha^2-\beta^2}\times\{\beta J_n(\alpha z)J_{n-1}(\beta z)-\alpha J_n(\beta z)J_{n-1}(\alpha z)\}$$

[see, *e.g.* Morse (1948), *p.* 188], and $J_n(k_{nm}a)=0$ by definition, we have

$$\mathbf{u}_{nm}(R,\Phi)=\frac{-2\pi k_{nm}ai^n}{(k_{nm}^2-4\pi^2R^2)}J_n(2\pi Ra)J_{n-1}(k_{nm}a)\exp(in\Phi)\,.$$

Rather than use the exponential, in practice it is more convenient to combine corresponding terms with positive and negative n, using

$$J_{-n}(x)=(-1)^nJ_n(x)$$

giving even ($\cos n\Phi$) and odd ($\sin n\Phi$) functions with $n\geq 0$.

In the $hk0$ projection of TMV protein the crystallographic symmetry is such that we need only consider the even functions ,and since we have taken the molecular centres to be at $\pm(\frac{1}{4},\frac{1}{4})$, it is necessary to include an additional phase factor i^{h+k}. Hence

$$\mathbf{u}_{nm(\mathrm{crystal})}(R,\Phi)=\frac{-4\pi k_{nm}ai^{n+h+k}}{(k_{nm}^2-4\pi^2R^2)}J_n(2\pi Ra)J_{n-1}(k_{nm}a)\cos(n\Phi)\,. \tag{9}$$

Again a separation into two parity groups is convenient, since $\mathbf{u}_{nm}$ must be real, and therefore for $(h+k)$ even only terms with n even contribute, and for $(h+k)$ odd only terms with n odd. More importantly, the above expression for the eigenvector applies even if neighbouring discs overlap, since it is simply a sum of transforms of individual discs, modified by appropriate phase factors.

The term $(k_{nm}^2-4\pi^2R^2)$ in the denominator of (9) implies that the significant contribution to the diffraction pattern from each eigenfunction is limited to a fairly small range of Bragg angles centred around $d^*=R=k_{nm}/2\pi$. Thus n and m can be chosen appropriately at any given resolution. The criterion used for this work was that when the $m_{\max}$th zero is fitted to the outer edge of the disc, the spacing between the $(m_{\max}-1)$ and $(m_{\max}+1)$th zeros of J_n should be approximately equal to the resolution used.

In addition, the eigenvectors $\mathbf{u}_{nm}$ must be normalized, so that

$$\sum_{\mathbf{h}}|u_{nm}(\mathbf{h})|^2=1$$

for all n,m. This can be done analytically since the eigenfunctions are orthogonal and satisfy

$$\int_0^a\int_0^{2\pi}J_n(k_{nm}r)\cos(n\Phi)J_{n'}(k_{n'm'}r)\cos(n'\Phi)r\mathrm{d}r\mathrm{d}\Phi=f_{nm}\delta_{nn'}\delta_{mm'}$$

where

$$f_{nm}=\int_0^{2\pi}\cos^2(n\Phi)\mathrm{d}\Phi\int_0^a J_n^2(k_{nm}r)r\mathrm{d}r=\tfrac{1}{2}\pi a^2J_{n-1}^2(k_{nm}a)\,.$$

In practice this orthogonality condition was used to put all the eigenvectors on the same scale, and the numerical scale factor was found by evaluating $\sum_{\mathbf{h}}|\mathbf{u}_{01}(\mathbf{h})|^2$ over a sufficiently wide range of $\mathbf{h}$.

Note that although $J_n(2\pi Ra)/(k_{nm}^2-4\pi^2R^2)$ becomes indeterminate when $R=k_{nm}/2\pi$, the quotient has no discontinuity, and so the limiting value

$$\underset{R\to k_{nm}/2\pi}{\mathrm{Lt.}}\frac{J_n(2\pi Ra)}{k_{nm}^2-4\pi^2R^2}=\frac{-a}{4\pi R}J_{n-1}(k_{nm}a)$$

may be used.

A comparison of the two methods

The eigenvector method has several practical advantages over computation with the matrix $\mathbf{H}$: since the $\mathbf{u}_j$ are computed analytically, there is no question of series-termination errors introduced by truncation of the G table. Thus electron-density maps generated by this method show no artificial drop in density level near the molecular boundaries. In addition, it is only necessary to store the matrix $\mathbf{A}$, which is smaller than $\mathbf{H}$ by a factor of $2N/m$. The most serious disadvantage of the eigenvector method is that the expansion functions will vary from problem to problem: in three dimensions, for example, the algebra is quite different, whereas the $\mathbf{H}$-matrix method is affected only insofar as the function G has a different form.

Results from the H-matrix method

The initial sign determination trials on TMV protein were carried out on only 200 reflexions from each parity group out of the 450 or so available at 6 Å resolution. This was partly to save computer time, and partly since it was felt that the sign determination would be more reliable at low resolution. The reflexions used

were chosen simply on the basis of low Bragg angle, without using any other criteria such as the value of |**F**|, so that the 200 reflexions correspond to a resolution of 9·5 Å.

The sign determination was carried out for the two parity groups quite separately, to avoid having to store a large matrix half of whose elements would be identically zero. The largest 150 coefficients of each equation were used, chosen on the basis of large values of $|F_{\mathbf{p}} \sum_{j=1}^{n} G(2\pi R_j a)|$, and arguments of G greater than $2\pi \times 2{\cdot}5$ were ignored. Later in the work it became clear that a considerably smaller maximum argument would suffice once the optimum envelope radius was known, although there is then a tendency for the least-squares method to behave irregularly, probably owing to the slow decrease of $\partial G/\partial a$ with increasing argument (Fig. 3).

An envelope radius of 90 Å was initially used, and in accordance with the results obtained from model structures, the electron-density map computed with the resulting signs showed a sharp drop in the mean density level beyond about 60 Å from the molecular centre. In addition, there is a tendency in the $(h+k)$ even parity group for density to appear at the centre of the ring, where it is known that there can be no protein. This density was excluded from subsequent calculations by using as the molecular envelope an annulus with inner radius 20 Å. All signs were made positive at the start of iteration, and reflexions added in blocks of 25, iterating at each stage until there were no further sign changes, this generally taking four or five cycles. At the end of the calculation, the residuals, defined by

$$R = \sum_{\mathbf{h}} |F_{\text{obs}} - F_{\text{calc}}| / \sum_{\mathbf{h}} F_{\text{obs}}$$

were 0·439 for the $(h+k)$ even parity group and 0·451 for $(h+k)$ odd. Subsequent work showed that the signs obtained were independent of the starting set, and also of the precise mode of iteration: the same result was obtained if the complete **F** vector was included from the start (Crowther, 1969).

Since allowing larger arguments of G is computationally difficult, a further trial was carried out, still using only 150 terms from each equation, but refining the envelope radius by the least-squares method after each

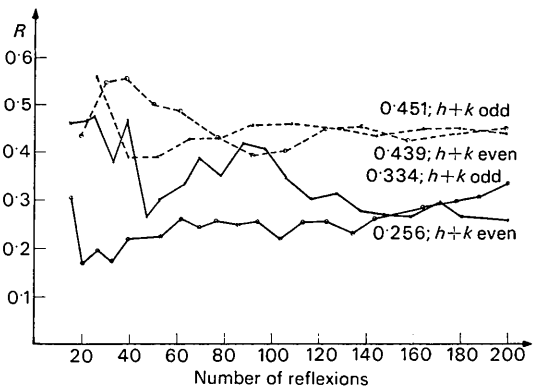

Fig. 4. Variation of R value with number of reflexions included in the phase equations. (-----): Envelope radius 90 Å; (——): envelope radius 110 Å.

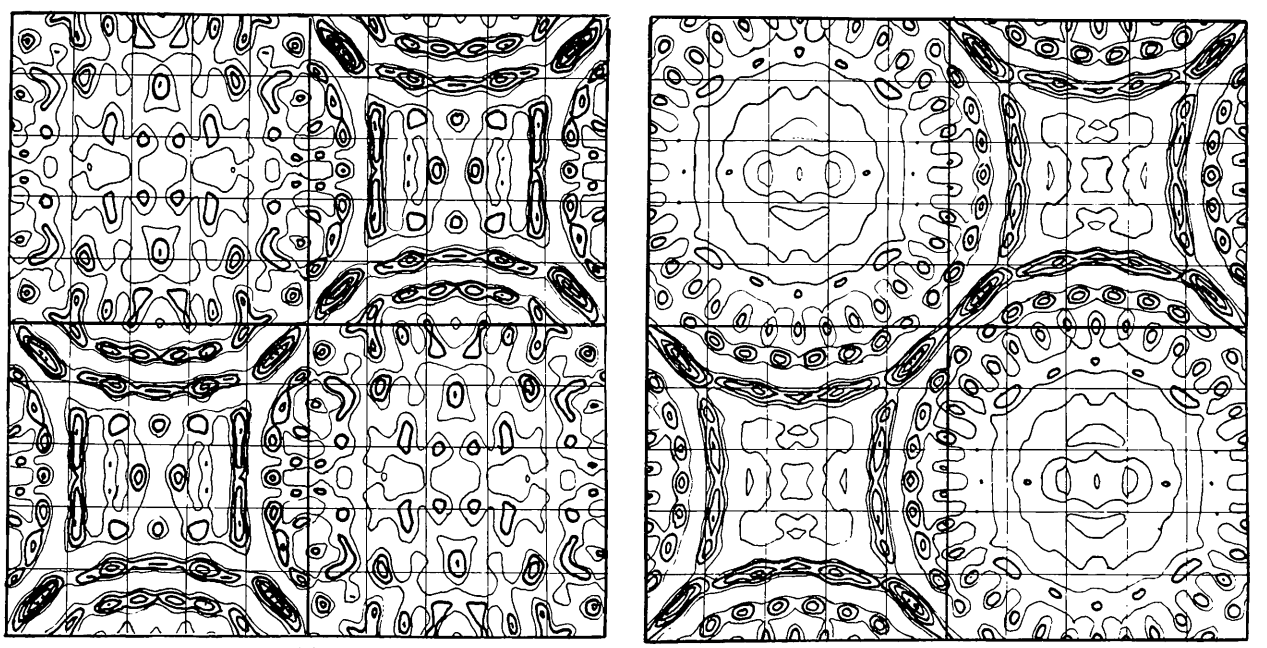

(*a*) (*b*)

Fig. 5. Comparison of 9·5 Å resolution $(h+k)$ even Fourier maps using signs obtained from (*a*) single isomorphous replacement, and (*b*) non-crystallographic symmetry.

block of 25 signs had iterated to completion. At the stage when 50 signs had been determined, the value of the radius increased to 110 Å, and remained stable at this value for the remainder of the calculation. The residual at the end of refinement was 0·256. On repeating the calculation for the reflexions with $(h+k)$ odd, the same value of 110 Å was obtained, and the final residual was 0·334. A plot of residual against number of reflexions included in the summation for $a=90$ Å and $a=110$ Å is shown in Fig. 4.

Comparison with isomorphous-replacement results

The signs obtained by Gilbert (1970) using the single isomorphous replacement method provide a valuable independent check of the results described above. On comparison, it was found that of the $(h+k)$ even parity group, 182 of the 200 signs determined from the non-crystallographic symmetry agreed with those found from isomorphous replacement. Of the 18 disagreements, 7 corrrespond to reflexions whose isomorphous figure of merit is less than 0·1, that is, reflexions whose signs are not reliably determined by this particular isomorphous replacement.

Fourier maps computed with the two sets of $(h+k)$ even signs are shown in Fig. 5. It can be seen that the principal differences between the two maps are at the centre of each disc and between the discs. This is not very surprising: firstly, the omission of unmeasurable low-order terms from the Fourier summation is expected to lead to some density in regions outside the discs, and secondly, no account has been taken of the solvent density outside the protein. The only effect of a uniform solvent density outside the molecular envelope is to change the low-angle intensities. The effect of this on the phase equations has been discussed by Main (1967), but since it only affects interactions with the $F(000)$ term (which was ignored in this work), no harm should result. The density fluctuations outside the protein annuli in Fig. 5(*a*) are therefore probably real features caused by non-uniform solvent density and omission of low-order reflexions from the summation. Omission of the $F(000)$ term also leads to an ambiguity in the overall sign of the electron density: all the signs could be wrong, but would still satisfy equation (1). The correct solution is the one which gives troughs but no high peaks outside the molecular envelopes.

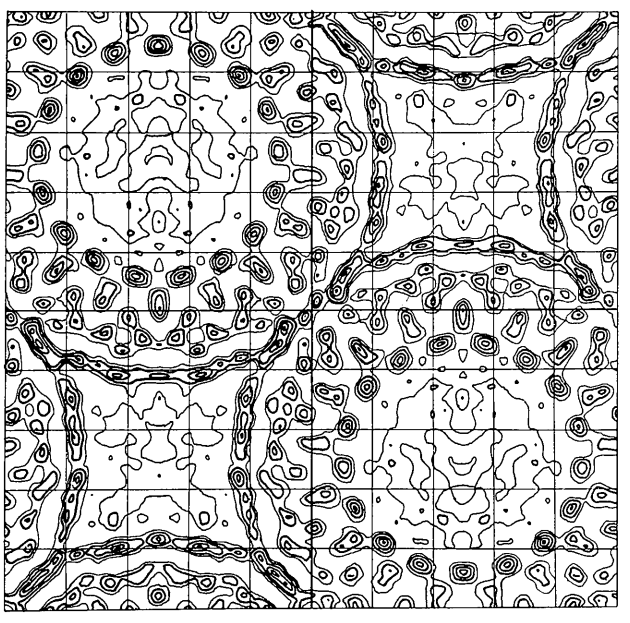

Fig. 6. 7 Å resolution Fourier map using 838 reflexions from both parity groups.

Comparison of the signs of reflexions belonging to the $(h+k)$ odd parity group showed much less striking agreement: only 120 of the 200 signs agreed with those found from isomorphous replacement, and the agreements appeared to be randomly distributed in reciprocal space. The reason for this soon became clear, however: the isomorphous derivative contains one mercury atom bound to each subunit, and the positions of binding, together with the relative azimuth of the two discs in the stack, result in the rings of mercury atoms having almost 34-fold symmetry in projection. Hence the heavy atoms alone form an almost face-centred arrangement in projection, and contribute little to the $(h+k)$ odd reflexions, resulting in unreliable sign determination.

Extension to higher resolution

Using the same envelope radius of 110 Å, the equations were set up for all reflexions out to 7Å resolution (425 with $h+k$ even and 413 with $h+k$ odd), this time allowing arguments of G up to $2\pi\times 2{\cdot}25$, and using the largest 200 coefficients of each equation. This corresponds to about 80% of the total information content of the equations, measured on the basis of $\sum_{\mathbf{p}}|H_{\mathbf{hp}}||F_{\mathbf{p(used)}}|/\sum_{\mathbf{p}}|H_{\mathbf{hp}}||F_{\mathbf{p(total)}}|$. The equations were solved in the same way as before, giving residuals of 0·290 for $(h+k)$ even and 0·353 for $(h+k)$ odd. Of the 425 reflexions in the even parity group, 355 agree with the isomorphous-replacement signs; although the agreement is not as good as at lower resolution, the two maps are very similar, and the agreement could no doubt be improved by using more coefficients and allowing larger arguments of G. Fig. 6 shows the map obtained using all 838 signs from both parity groups.

Results from the eigenvector method

In the first calculation using the eigenvector method, 19 functions (16 J_0's and 3 J_{34}'s) were used to describe the structure to 9·5 Å resolution, using $(h+k)$ even reflexions only. Table 1 shows the norms of these eigenvectors, evaluated over the set of observed reflexions. Convergence was complete in five cycles, giving a residual

of 0·48. Of the 200 signs determined, 172 agreed with those obtained from isomorphous replacement. Omission of the four lowest-order J_0 functions, which contribute significantly only to the low-order reflexions and are not orthogonal over the limited range of reflexions considered, gave a residual of 0·35, and 169 agreements with isomorphous replacement. On extending this calculation to higher (7Å) resolution, a residual of 0·42 was obtained using 30 functions. Despite this rather high value, the principal features of the Fourier map agree with those in Fig. 6. The higher residual is presumably due to the non-orthogonality of some of the higher order functions over a limited resolution range, leading to eigenvalues of $\mathbf{A}\tilde{\mathbf{A}}^*$ less than unity. The corresponding eigenvectors are subsequently weighted down by the iteration process.

Table 1. *Norms of the eigenvectors* $(h+k$ *even*) *used to describe the structure to* 9·5 Å *resolution*

The squares of these norms are the 'allowed' eigenvectors of the matrix $\mathbf{A}\tilde{\mathbf{A}}^*$. All other eigenvectors were less than 10^{-4}.

m	$n=0$	m	$n=0$	m	$n=0$	m	$n=34$
1	0·0006	7	0·7168	12	0·9839	1	0·9506
2	0·0017	8	0·8099	13	0·9773	2	0·9518
3	0·0052	9	0·9673	14	0·9444	3	0·9371
4	0·0164	10	0·9780	15	0·9618		
5	0·1074	11	0·9822	16	0·9540		
6	0·7144						

Application of this phasing procedure to the reflexions with $(h+k)$ odd is more interesting. An attempt to determine signs at 7Å resolution using 31 eigenfunctions (21 J_{17}'s and 10 J_{51}'s, Table 2) gave a residual of 0·37, and the Fourier map shown in Fig. 7. When the signs (arranged in order of increasing Bragg angle) were compared with those found using the **H**-matrix method, it was found that the two sets matched almost perfectly *in bands*, but at various points in reciprocal space there was a changeover from total agreement to total disagreement. A possible reason for this is as follows: for reflexions with $(h+k)$ odd and $l=0$, the structure factor $F_{\mathbf{h}}$ is given by

$$F_{\mathbf{h}} = 136 \sum_j \sum_n f_j i^n J_n(2\pi R r_j) \cos(n\varphi_j) \cos(n\Phi)$$

(Gilbert, 1970), where r_j, φ_j are polar positional coordinates of atom j; R, Φ are polar coordinates of the reciprocal-lattice point h,k, and $n=17$, 51 *etc.* Thus the continuous transform has a series of diametrical nodes where $n\Phi = \pm\pi/2$. Inside any sector between two nodes, the radial variation of the transform depends on the unknown r_j's, but there will generally be some nodes and regions of small $|\mathbf{F}|$. Now in order for the solution generated by the matrix **H** to have 17-fold symmetry, the calculated F's must change sign correctly at the diametrical nodes (*i.e.* on going round a ring at fixed R), but it is possible to introduce incorrect sign changes along a radial line in reciprocal space (*i.e.* a line of constant Φ) without destroying the 17-fold symmetry. Moreover, the agreement between F_{obs} and $|\mathbf{F}_{calc}|$ will still be good, except near the nodes of the transform. This is exactly the behaviour observed, and it is a consequence of the iteration method that the problem arises; we should really fit the *small* amplitudes as accurately as possible: although these make negligible contributions to the signs of the large amplitudes when substituted into the phase equations, they are important in that they eliminate a large number of solutions (Vainshtein & Kayushina, 1967).

Table 2. *Norms of the eigenvectors* $(h+k$ *odd*) *used to describe the structure to* 7 Å *resolution*

m	$n=17$	m	$n=17$	m	$n=51$
1	0·9383	12	0·8654	1	0·6631
2	0·9286	13	0·8354	2	0·9331
3	0·8776	14	0·8583	3	0·8102
4	0·8675	15	0·8606	4	0·8368
5	0·9039	16	0·8468	5	0·8742
6	0·9028	17	0·8526	6	0·2191
7	0·8858	18	0·4215	7	0·4461
8	0·9184	19	0·4684	8	0·2031
9	0·8831	20	0·2578	9	0·2459
10	0·8702	21	0·1798	10	0·1690
11	0·8776				

Thus in the resolution range where only J_{17} terms contribute to the diffraction pattern, the problem reduces to the one-dimensional one of determining whereabouts on a radial line the sign changes occur. The only condition which the resulting calculated transform must obey is the rather weak one that its

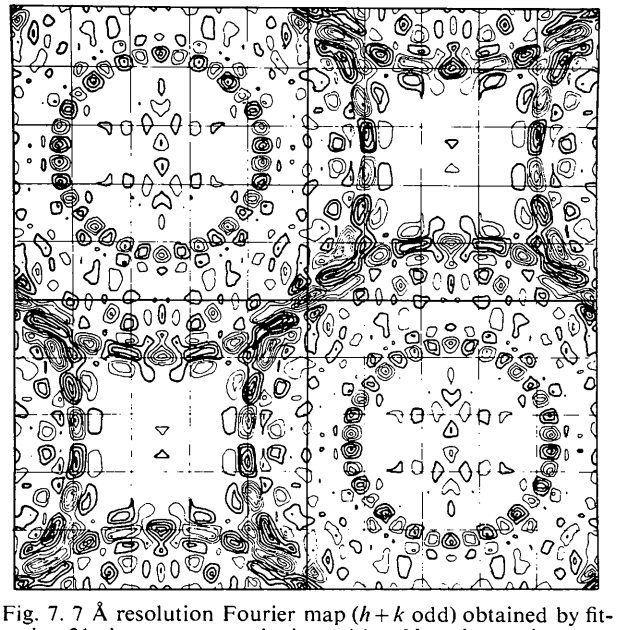

Fig. 7. 7 Å resolution Fourier map $(h+k$ odd) obtained by fitting 31 eigenvectors to the intensities. Negatioe regions are represented by light contours.

transform must be bounded by the envelope containing the molecule (Bragg & Perutz, 1952). Since direct calculation of the eigenvectors imposes this boundary condition rather more rigorously than the **H**-matrix method, it is probable that the $(h+k)$ odd sign set derived by this new method is the better of the two. Inspection of the two Fourier maps tends to support this proposal: the map obtained from the **H**-matrix iteration shows a ring of high density at a radius of 60 Å and little else; the map obtained by the eigenvector method (Fig. 7) shows a more even distribution of density extending right out to 90 Å. Further evidence that the signs are correct is found from comparison with the isomorphous replacement signs as a function of the isomorphous figure of merit m. All 14 signs with $m \geq 0{\cdot}6$ agree with those found by direct calculation of the eigenvectors. As m decreases, so does the percentage agreement, until for $m \leq 0{\cdot}2$ it is effectively random. These results are presented in histogram form in Fig. 8, which shows the percentage agreement (*a*) between SIR signs and those obtained by the eigenvector method, and (*b*) between SIR signs and those found by **H**-matrix iteration. The figure in each box of the histogram gives the number of sign agreements in that range of m. (The apparent discrepancies in the figures for $m \leq 0{\cdot}3$ arise because the eigenvector calculation was extended to a marginally higher resolution than the **H**-matrix calculation.)

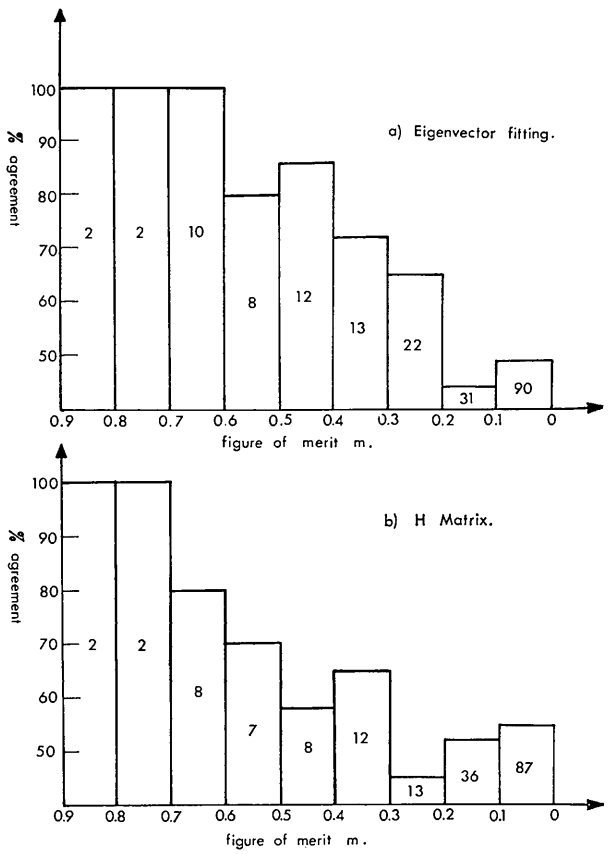

Fig. 8. Comparison of signs $(h+k$ odd) obtained from non-crystallographic symmetry and single isomorphous replacement. (*a*) Eigenvector fitting; (*b*) **H** matrix.

That block-switching effects do not occur in the $(h+k)$ even case may be attributed to the fact that the transform contains strong cylindrically symmetric contributions from the J_0 terms, on which the J_{34} terms act as a perturbation. The J_0 contribution effectively means that there is no sign ambiguity at low resolution, so that the first few signs determined by the **H**-matrix method are invariably correct, and correct sign indications are propagated through reciprocal space. In the $(h+k)$ odd case, J_{17} terms start contributing only at a resolution of about 35 Å. There is then a possibility of some incorrect signs being determined at the start of the iteration and this incorrect starting set will generate wrong signs at higher resolution.

Confirmation that the signs obtained using the eigenvector method are essentially correct has been provided by Drs J. N. Champness and T. C. C. Tao of this laboratory, who have used them to compute difference-Fourier maps of new heavy-atom derivatives of TMV protein. These maps all show rings of 17 heavy atom peaks, but have fewer spurious peaks than the corresponding maps computed with the currently available SIR signs.

Conclusions

The results described here clearly show that the use of non-crystallographic symmetry for phase determination can give meaningful results for a real protein structure with high symmetry. There seems to be no reason why this method should not be extended into three dimensions: the fact that the phases can take only two possible values in projection has no doubt helped in the present work, but the results quoted by Main (1967) and Crowther (1969) leave little doubt that the high degree of non-crystallographic symmetry in TMV protein is sufficient to obtain good three-dimensional phases *ab initio*. A high-resolution structural study of this protein raises many technical problems on account of the large unit cell. Nevertheless, the system is ideal for attempting a direct solution of the phase problem.

I should like to thank Drs D. M. Blow, R. A. Crowther, R. Diamond and A. Klug for their many valuable suggestions during the course of the work and preparation of the manuscript. I am most grateful to Drs P. F. C. Gilbert and J. N. Champness for allowing me to use their X-ray data, and for putting the results to the test in their difference-Fourier calculations. All computing was done on the IBM360/44 computer at the Institute of Theoretical Astronomy, Cambridge. and I thank the staff for their assistance.

This work forms part of a Ph. D. thesis submitted to Cambridge University, and was carried out during the tenure of a Medical Research Council Scholarship for training in research methods.

References

BRAGG, W. L. & PERUTZ, M. F. (1952). *Proc. Roy. Soc.* A**213**, 425–435.
CASPAR, D. L. D. (1963). *Advanc. Protein Chem.* **18**, 37–121.
CROWTHER, R. A. (1967). *Acta Cryst.* **22**, 758–764.
CROWTHER, R. A. (1968). Ph. D. thesis, Univ. of Cambridge.
CROWTHER, R. A. (1969). *Acta Cryst.* B**25**, 2571–2580.
CROWTHER, R. A. & AMOS, L. A. (1971). *J. Mol. Biol.* **60**, 123–130.
FINCH, J. T. & KLUG, A. (1971). *Phil. Trans.* B**261**, 211–219.
FINCH, J. T., LEBERMAN, R., YU-SHANG, C. & KLUG, A. (1966). *Nature, Lond.* **212**, 349–350.
FRANKLIN, R. E. & HOLMES, K. C. (1958). *Acta Cryst.* **11**, 213–220.
GILBERT, P. F. C. (1970). Ph. D. thesis, Univ. of Cambridge.
JAMES, R. W. (1948). *The Optical Principles of the Diffraction of X-rays*. London: Bell.
KLUG, A. & DURHAM, A. C. H. (1971). *Cold Spring Harbor Symposia on Quantitative Biology*, Vol. XXXVI, pp. 449–460.
MAIN, P. (1967). *Acta Cryst.* **23**, 50–54.
MAIN, P. & ROSSMANN, M. G. (1966). *Acta Cryst.* **21**, 67–72.
MORSE, P. M. (1948). *Vibration and Sound*. New York: McGraw-Hill.
PATTERSON, A. L. (1939). *Phys. Rev.* **56**, 972–978.
ROSSMANN, M. G. & BLOW, D. M. (1962). *Acta Cryst.* **15**, 24–31.
ROSSMANN, M. G. & BLOW, D. M. (1963). *Acta Cryst.* **16**, 39–45.
ROSSMANN, M. G. & BLOW, D. M. (1964). *Acta Cryst.* **17**, 1474–1475.
TOLLIN, P. & ROSSMANN, M. G. (1966). *Acta Cryst.* **21**, 872–876.
VAINSHTEIN, B. K. & KAYUSHINA, R. L. (1967). *Sov. Phys. Crystallogr.* **11**, 468–474.
WATSON, J. D. (1954). *Biochim. Biophys. Acta*, **13**, 10–19.

Acta Cryst. (1973). A**29**, 554

A Lattice-Dynamical Interpretation of Molecular Rigid-Body Vibration Tensors

BY C. SCHERINGER*

Institut für Kristallographie der Universität, Karlsruhe, Germany (BRD)

(*Received* 6 *March* 1973; *accepted* 30 *March* 1973)

The rigid-body motions of molecules in crystals are treated with the aid of lattice dynamics of molecular crystals. An equation is derived in which the rigid-body vibration tensors **TLS** are related to the dynamical matrices of the crystal. Then the components of **TLS** are explicitly given in lattice-dynamical terms. A procedure is developed with which the trace of **S**, which cannot be determined from diffraction data, can be approximately determined. The principal motions of the rigid-body vibrations of molecules are discussed. Which types of coordinate systems can be used to give a physically meaningful description of the rigid-body motions is examined from a dynamical point of view. A 'dynamical' interpretation of the tensors **TLS** is given which consists in relating **TLS** to the intermolecular forces of the crystal and then comparing the intermolecular forces with the packing of the molecules in the crystal. The interpretation is illustrated with the structures of maleic anhydride and 5-chloro-1,4-naphthoquinone.

1. Introduction

Cruickshank (1956*a*) was the first to show how the external vibrations of almost rigid molecules can be described by two tensors **T** and **L** which account for the translations and librations of the molecules respectively. However, Schomaker & Trueblood (1968) showed that, in general, the rigid-body motions are fully accounted for only if a (translation–libration) correlation tensor **S** with 9 components is introduced. Only 8 of these components can be determined from diffraction data. Schomaker & Trueblood's derivation was performed in geometrical and statistical terms, *cf.* also Johnson (1970). In connexion with their derivation Schomaker & Trueblood discuss (geometrical) possibilities for the actual rigid-body motions. In the main these authors consider a model in which the molecule carries out six uncorrelated simple motions; three of them are screw motions about perpendicular non-intersecting axes, and three are pure translations. Although no claim is expressed '... that the elementary motions so derived must have dynamic significance' (Johnson, 1970) the rigid-body motions described by the non-intersecting-axes model are related to the geometrical (and chemical) arrangement of the molecules in a given structure; *cf.* also the discussion of the rigid-body motions of the glycolic acid molecule as given by Ellison, Johnson & Levy (1971). This means that the screw motions about non-intersecting axes are

* Present address: Fritz-Haber-Institut der Max-Planck-Gesellschaft, D–1000 Berlin 33, Faradayweg 4-6, Germany.